Available online at www.sciencedirect.com
SCIENCE DIRECT®
Nuclear Instruments and Methods in Physics Research A 543 (2005) 306–311
NUCLEAR INSTRUMENTS & METHODS IN PHYSICS RESEARCH Section A
www.elsevier.com/locate/nima

The live lattices become visible in coherent synchrotron X-rays

V. Kohn[a], C. Rau[b], P.M. Sergienko[c,*], I. Snigireva[b], A. Snigirev[b], A. Vazina[c]

[a]*Russian Research Centre "Kurchatov Institute", 123182, Moscow, Russian Federation*
[b]*European Synchrotron Radiation Facility, BP-220, F-38043, Grenoble, France*
[c]*Institute of Theoretical and Experimental Biophysics, RAS, 142290 Pushchino, Russian Federation*

Available online 10 March 2005

Abstract

We demonstrate a great potential of the method of phase contrast imaging for a study of muscles and animal organism in normal and pathological states. The method is applied to image biological tissues that have the unique feature of structure–translation symmetry of 0.1–10 μm periodicity. The cross-striated muscle is the most interesting example of such objects. The experiment was done using high-brilliant coherent X-rays, delivered by synchrotron radiation source of third generation (ESRF, Grenoble), and high-resolution 2D-detector.

PACS: 41.60.Ap; 61.10.−i; 87.22.Jb

Keywords: Synchrotron radiation; Phase contrast imaging; Skeletal muscle

1. Introduction

Recently, a new technique of phase contrast imaging of transparent objects with high-energy coherent X-rays was applied, and it is currently under extensive development. Three various approaches were tested, which are based on single-crystal interferometry [1,2], single-crystal collimation [3–5] and in-line setup with synchrotron radiation sources [6–9] or microfocus X-ray tubes [10,11]. The synchrotron radiation sources of third generation offer such a possibility due to its quite high transverse spatial coherence [12], which results from a very small transverse source size (about tens of microns) and a large source-to-object distance (more than 50 m). The necessary longitudinal coherence is easily obtained with a single-crystal monochromator. Under these conditions, the theoretical resolution of the image at the object-to-detector distance of the order of 10 cm is smaller than 1 μm. It was shown [6] that a weak phase contrast (visibility) of the object image in the Frenel region of diffraction is comparable to a value of the phase shift variation produced by the object. For X-ray energy higher than 10 keV the decrement of refractive index for light elements

*Corresponding author. Tel.: +7 0967 739 143; fax: +7 0967 330 553.
E-mail address: serg@iteb.ru (P.M. Sergienko).

0168-9002/$ - see front matter © 2005 Elsevier B.V. All rights reserved.
doi:10.1016/j.nima.2005.01.246

like carbon is 1000 times larger than the index of absorption. Therefore it is obvious, the phase contrast is much more sensitive than the absorption contrast.

This is why the technique of phase contrast imaging is very useful in biological and medical studies. It reduces potential damage of the tissues due to considerably reduced absorbed dose, as compared to the absorption imaging. The high resolution of this technique allows to make visible a fine structure of the optical density of living organisms, in particular, periodical variation of the density in muscles with a period of a few microns (see Fig. 1). In this article, we report the first successful attempt to record the phase contrast images of living cross-striated skeletal muscles of *Rana ridibunda*.

2. Materials and method

A schematic structure of the skeletal muscle fiber is shown on Fig. 1(a). Such fibers are built of several hundreds of parallel myofibrils. An elementary contracting unit of myofibril is a sarcomere shown in Fig. 1(b) and (c) between two Z-membranes. Each myofibril may include up to two thousand series-connected identical sarcomeres. Each sarcomere contains the ordered structure of two interpenetrating sets of filaments. Located in the middle of sarcomere thick filaments set is constituted mainly from myosin. Two sets of thin filaments are attached to Z-membranes and are mainly constituted from actin. During muscle contraction and stretching, the change of sarcomere length is realized by means of mutual sliding of thick and thin filaments relative to each other without changing filaments lengths. Fig. 1 shows schemes for two sarcomere lengths: panel (b)—muscle in the rest state, sarcomere length from 2.2 to 2.5 μm, thick and thin filament lattices are overlapped partially; panel (c)—muscle stretched up to the sarcomere length 3.65 μm, thick and thin filament lattices have no overlap.

In skeletal muscles, Z-membranes of neighboring myofibrils are lined up in register so that the skeletal muscle fiber image in the optical microscope has the characteristic striated picture. That is why skeletal muscles are usually named as cross-striated muscles.

The experiment has been done at the ID 22 beamline of the European Synchrotron Radiation Facility. A sketch of the experimental setup is shown in Fig. 2. A high-resolution X-ray CCD FRELON camera was used as a detector. The X-ray energy, selected by the monochromator, was set to 20 keV. The source-to-object distance was 62 m whereas the transverse source size was estimated as 30 μm. The detector was placed at 10 cm from the sample in order to get good compromise between contrast and resolution. Exposure time varied from 5 to 10 s.

Various muscles of *Rana ridibunda* frog at rest and during contraction and stretching were studied. Separated muscles as well as the intact frog leg samples were investigated. The thickness of isolated muscles was varied from 1 to 4 mm. *Sartorius* muscle, *Gastrocnemius* muscle, *Lumbricalis Longus* and *Lumbricalis Brevis* of IV and V digit were taken at the rest length. In *Semitendinosus* muscle samples, the dorsal head was kept at the rest length whereas the ventral head was stretched to no overlap. Both heads were displayed on the same image simultaneously.

The intact frog leg samples had diameter about 10 mm. The X-ray beam passes through the both layers of skin and throughout the muscle; therefore, sometimes the moiré patterns of skin were also observed. Fig. 3 shows three experimental images of I (actin) and A (myosin) bands of *Sartorius* muscle at various sarcomere length. The panels A, B and C show the random fragments of images with the periods of 2.2, 3.0 and 4.0 μm, respectively. The sarcomere length was controlled by the method of laser optical diffraction ($\lambda = 0.570\,\mu m$). Note, the absolute value of contrast (visibility) has been found to be small (about 3%). This simplifies the problem of calculating the phase shift variation from the intensity variation as shown below.

3. The theory of weak phase-contrast imaging

Homogeneous coherent X-ray wave is detected as a homogeneous intensity profile. The wave is

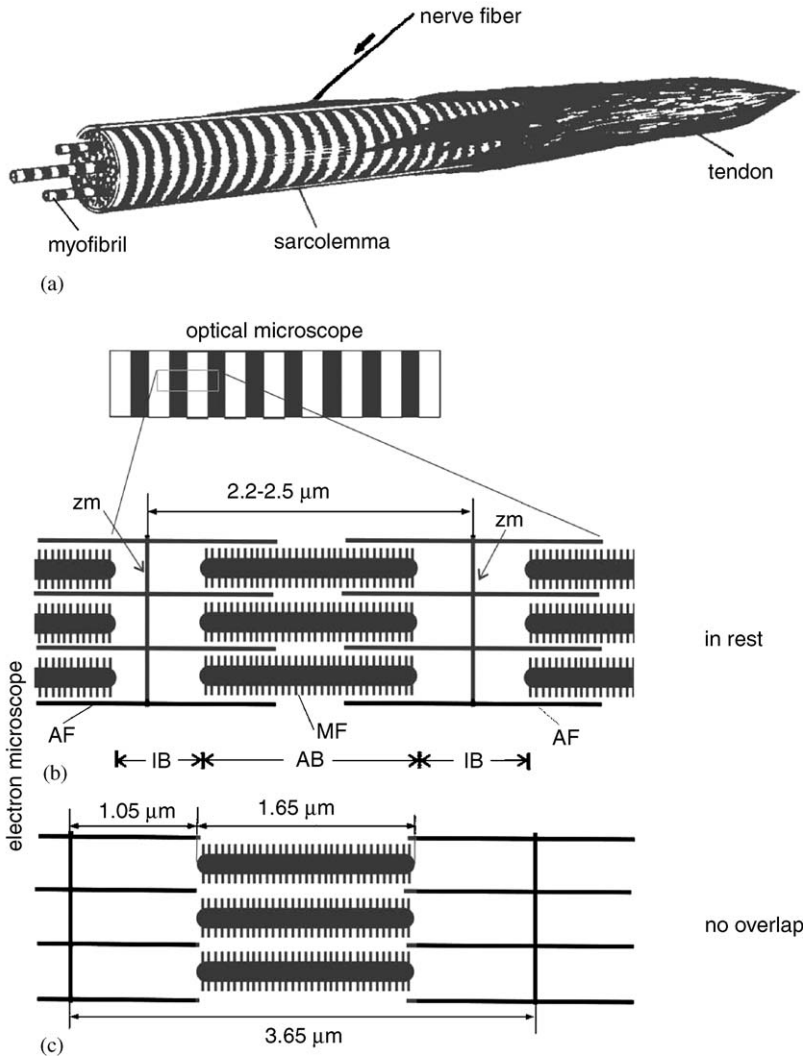

Fig. 1. A schematic structure of the skeletal muscle: (a) the part of muscle fiber; a muscle tendon, a nerve termination, a transparent muscle sheath (sarcolemma) and separated muscle fibrils (myofibrils) are shown; (b) the scheme for explaining appearance of cross-striation in muscle under observation in the optical (top) and electron (bottom) microscopes; ZM—Z-membrane; AF—thin (actin) filament; MF—thick (myosin) filament; IB—clear (isotropic) band; AB—dark (anisotropic) band; (c) the scheme of electron microphotography of the same muscle sarcomere stretched up to the length when thick and thin filament lattices have no overlap; lengths of thick and thin filaments are indicated.

modulated by the object in such a way that both the amplitude and the phase of the wave become uneven in space. The amplitude modulation occurs due to X-ray absorption in matter. Such a modulation can be detected immediately. The phase modulation occurs due to a difference of speed of light in matter compared to the empty space. The phase cannot be detected if the intensity is registered just after the object. However, at some distance from the object the phase modulation leads to the intensity modulation due to a propagation of coherent wave in space. Such an intensity modulation depends not only on the phase profile but also on the distance from the object.

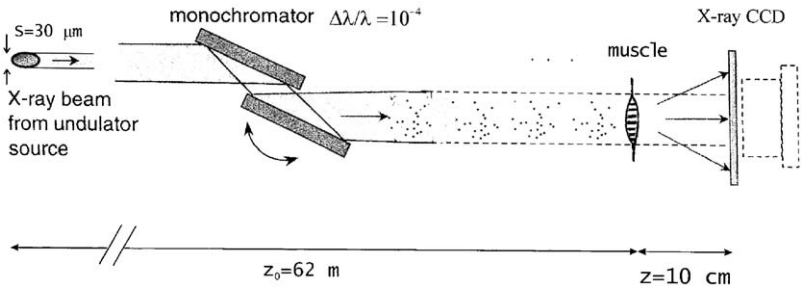

Fig. 2. An experimental setup at the ID 22 beamline at the ESRF. Source size $s = 30\,\mu m$; source divergence $30 \times 20\,\mu\cdot^2$; flux density 10^{13} ph/s/mm^2; energy 20 keV; source-to-sample distance 62 m; beam size on the sample $1.5 \times 1.3\,mm^2$; sample-to-detector distance 10 cm.

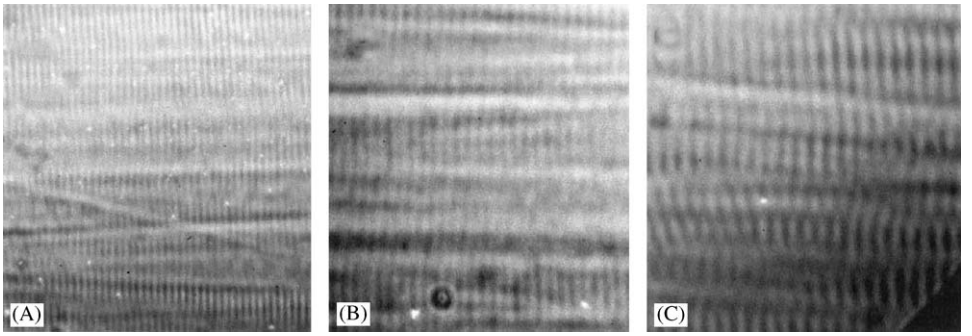

Fig. 3. The X-ray phase contrast imaging of living cross-striated skeletal *Sartorius* muscle of frog *Rana ridibunda*: (A) in rest, sarcomere length 2.2 μm; (B) after stretching to the sarcomere length 3 μm; (C) stretched to no overlap, sarcomere length 4 μm.

The propagation of the coherent wave through the thin object, having one-dimensional transverse variation of the optical density, is described by the complex transmission amplitude

$$f(x) = \exp\left(-i\,\frac{2\pi}{\lambda}\int dz[\delta(x,z) - i\beta(x,z)]\right) \qquad (1)$$

where λ is a wavelength, z is a coordinate along the optical axis, x is a coordinate across the X-ray beam, $\delta(x,z)$ is a local decrement of refractive index for a object, $\beta(x,z)$ is a local index of absorption.

Assuming the object to be illuminated by a spherical wave from the point source located at the distance z_0 from the object, we calculate the intensity at the distance z_i after the object. It is usual for in-line experimental setup that the longitudinal distances are much larger than the transverse distances, so that the paraxial approximation is valid. The normalized intensity profile $I_n(x') = |a(x_0)|^2$ where $x_0 = x'z_0/z_t$ is a projection of the point at the detector to the object plane, $z_t = z_0 + z_i$. The correspondence between the functions $f(x)$ and $a(x_0)$ is given by a convolution with the total propagator

$$a(x_0) = \int dx\, P(x_0 - x, z_r) f(x) \qquad (2)$$

where

$$P(x,z) = \frac{1}{(i\lambda z)^{1/2}} \exp\left(i\pi\,\frac{x^2}{\lambda z}\right), \quad z_r = \frac{z_0 z_i}{z_t}. \qquad (3)$$

In general case the correspondence between the phase of the transmission amplitude $f(x)$ and the intensity $I_n(x')$ is rather complicated. Therefore, the problem of the phase reconstruction from the

measured intensity distribution is not simple. However, in the case of weak and pure phase contrast the problem becomes single-valued and more simple. Let us assume that

$$f(x) = I_f^{1/2} \exp(i\varphi_0) \exp[i\Delta\varphi(x)] = f_0 \exp[i\Delta\varphi(x)] \quad (4)$$

where the absorption is constant, φ_0 is a mean phase shift. Note, that for pure transparent object $I_f = 1$. If $|\Delta\varphi(x)| \ll 1$, we can expand the expression for the intensity profile $|a(x_0)|^2$ as a power series in $\Delta\varphi(x)$ and keep only the first term.

As a result we obtain

$$V(x_0) = \frac{I_n(x') - I_f}{I_f} \approx \int dx\, Q(x_0 - x, z_r)\Delta\varphi(x). \quad (5)$$

We shall call the function $V(x)$ as a local visibility of image. Here

$$Q(x,z) = i[P(x,z) - P^*(x,z)] = \frac{1}{(\lambda z)^{1/2}} \sin\left(\pi \frac{x^2}{\lambda z} + \frac{3}{4}\pi\right). \quad (6)$$

Thus, we have a linear connection between the measured visibility profile and the phase shift profile. Note, our approach is similar to the one proposed in Ref. [13], but is developed for a divergent beam and large values of mean absorption and phase.

Since the integral in Eq. (5) is a convolution, the solution can be obtained by double Fourier transformation. The Fourier image of the propagator is

$$Q(q,z) = 2\sin\left(\frac{\lambda z}{4\pi} q^2\right). \quad (7)$$

It can take zero values; therefore, some regularization procedure is necessary. It is convenient to use the method proposed by Nugent [14], namely,

$$\Delta\varphi(q) = \frac{V(q)Q(q,z_r)}{[Q^2(q,z_r) + \varepsilon]} \quad (8)$$

where ε is a small parameter. Here, the numerator corresponds to the standard optical reconstruction algorithm while the denominator is necessary for a solution of the twin-image elimination problem.

4. Discussion

As follows from Eq. (1), the phase of the complex transmission amplitude is equal to an integral value of the local decrement of refractive index. The latter is proportional to the local electron density of the object under study. The knowledge of the phase allows one to reconstruct the electron density by means of standard tomographic technique. We apply the method of the phase reconstruction described above to the experimental images of the frog leg muscles. Fig. 4 shows two examples of calculation. The parameters of the calculation correspondent to experimental conditions. The panel (a) of Fig. 4 shows the model phase variation profile which may be assigned to the object having a grid on the surface with a period of 2 μm. The calculated local visibility profile is shown in the panel (b).

As was pointed out in Ref. [6], the mean value of the local visibility variation is proportional to the

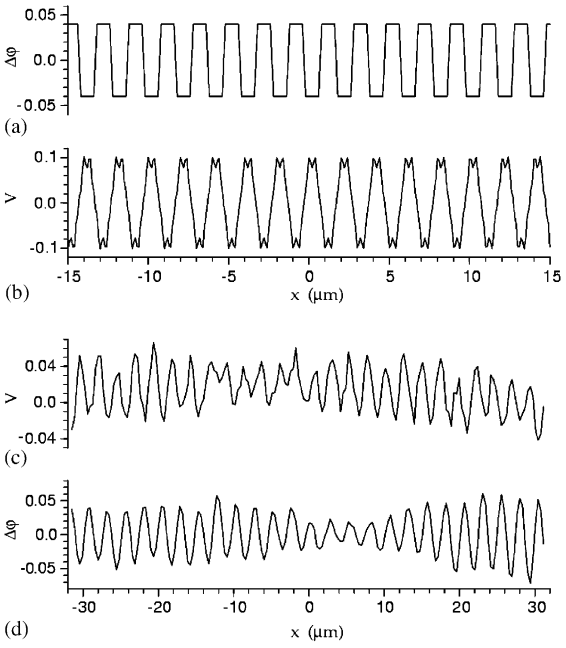

Fig. 4. The results of computer simulations: (a) the model object phase variation profile with the period 2 μm; (b) the calculated local visibility profile; (c) a random fragment of the experimental intensity profile of the *Sartorius* muscle from the panel A of Fig. 3; (d) the reconstructed phase variation profile.

mean value of the phase variation, and the proportionality coefficient is close to unity for most of distances. However, there may be specific distances z_r where the visibility is smaller or larger. As follows from Eq. (4), a sinusoidal phase shift variation, $\Delta\varphi(x) = a\sin(2\pi x/p)$ with $a \ll 1$, leads to the sinusoidal local visibility profile $V(x) = 2a\sin(\pi\lambda z_r/p^2)\sin(2\pi x/p)$ with the same period and the modified amplitude. This means that the amplitudes of different harmonics of arbitrary periodical profile become modified by different factors. As a result, one can obtain the periodical visibility with a different shape. When $\lambda z_r = Np^2$, where N is an integer, the visibility is equal to zero as a consequence of the Talbot effect [15]. Therefore, it is evident that one must vary the distance from the object to obtain the better local visibility variation. On the other hand, the computer reconstruction procedure is necessary to obtain the real phase variation profile produced by the object.

As follows from Fig. 4(a) and (b), the distance 10 cm is proper because the local visibility variation is twice as larger than the phase variation. The Fig. 4(c) shows the random fragment of the experimental visibility from the panel A of Fig. 3 with the mean period of 2.2 μm. The reconstructed phase variation profile is shown in Fig. 4(d). The regularization parameter $\varepsilon = 0.04$ was used in the calculation. As follows from the reconstruction, the periods of variation of the image visibility and the phase profile for the transmission amplitude of the object are close to each other whereas the shapes of profiles are apparently different.

5. Conclusion

We have obtained for the first time the direct phase contrast images of the fine periodical structure of the matter density of live frog muscles with the resolution better than the fraction of a micron. Despite of the small visibility of the images, the structures are clearly seen. On the other hand, the small value of phase shift variation allows us to make a straightforward reconstruction of the phase variation profile from the local visibility profile. This opens a possibility to obtain a real distribution of the matter density inside the object by standard tomographic technique. Combination of phase contrast imaging with micro-diffraction and micro-spectroscopy has a great potential for biological research. High-energy introscopy allows one to make introvital studies of the animal organism in normal and pathology states.

Acknowledgments

The work was supported by RFBR Grant nos. 02-02-16836, 03-02-17409, 04-02-17389.

References

[1] A. Momose, Nucl. Instr. and Meth. A 352 (1995) 622.
[2] A. Momose, J. Synchr. Radiat. 9 (3) (2002) 136.
[3] V.A. Somenkov, A.K. Tkalich, S.Sh. Shilshtein, Sov. Tech. Phys. 36 (1991) 1309.
[4] V.N. Ingal, E.A. Beliaevskaya, J. Phys. D 28 (1995) 2314.
[5] T.J. Davis, D. Gao, T.E. Gureyev, A.W. Stevenson, S.W. Wilkins, Nature 373 (1995) 595.
[6] A. Snigirev, I. Snigireva, V. Kohn, S. Kuznetsov, I. Schelokov, Rev. Sci. Instr. 66 (12) (1995) 5486.
[7] K.A. Nugent, T.E. Gureyev, D.F. Cookson, D. Paganin, Z. Barnea, Phys. Rev. Lett. 77 (14) (1996) 2961.
[8] P. Cloetens, R. Barrett, J. Baruchel, J.-P. Guigay, M. Schlenker, J. Phys. D 29 (1996) 133.
[9] P. Spanne, C. Raven, I. Snigireva, A. Snigirev, Phys. Med. Biol. 44 (1999) 741.
[10] R. Fitzgerald, Phys. Today 53 (7) (2000) 23.
[11] T.E. Gureyev, S. Mayo, S.W. Wilkins, D. Paganin, A.W. Stevenson, Phys. Rev. Lett. 86 (25) (2001) 5827.
[12] V. Kohn, I. Snigireva, A. Snigirev, Phys. Rev. Lett. 85 (13) (2000) 2745.
[13] A. Pogany, D. Gao, S. Wilkins, Rev. Sci. Instr. 68 (1997) 2774.
[14] K.A. Nugent, Opt. Commun. 78 (1990) 293.
[15] F. Talbot, Philos. Mag. 9 (1836) 401.